Oil Shale, 2014, Vol. 31, No. 2, pp. 161–173
doi: 10.3176/oil.2014.2.06
ISSN 0208-189X


# REMOVAL OF METHYLENE BLUE FROM AQUEOUS SOLUTION BY USING OIL SHALE ASH

ZENGYING ZHAO[(a)], JIANGYAN YUAN[(b)], MENG FU[(b)], LA SU[(b)], ZHAOHUI LI[(b,c)*]

[(a)] School of Science, National Laboratory of Mineral Materials, China University of Geosciences (Beijing), Beijing 100083, P.R. China
[(b)] School of Materials Science and Technology, China University of Geosciences (Beijing), Beijing 100083, P.R. China
[(c)] Department of Geosciences, University of Wisconsin–Parkside, 900 Wood Road, Kenosha, WI 53144, USA

***Abstract.*** *Oil shale ash (OSA) is a solid waste from the production process of shale oil. The large quantity of OSA generated in China yearly has led to serious, difficult-to-solve environmental problems. With a view to reducing OSA-induced environmental pressure, in this study, removal of methylene blue (MB) from aqueous solution by using OSA was investigated at different physical and chemical parameters, such as pH, temperature, initial MB concentration, and contact time. The experimental results showed that both the Langmuir and Freundlich models fitted the MB adsorption data well with an adsorption capacity as high as 250 mg/g. Removal of MB by OSA was relatively fast and equilibrium could be achieved in 2 h. Adsorption of MB by OSA was an endothermic reaction, and the change of free energy after MB adsorption indicated physical adsorption in nature. The results suggest a new potential utilization of OSA for the removal of color dye from wastewater.*

***Keywords:*** *adsorption, dye, methylene blue, removal, oil shale ash.*

## 1. Introduction

Mining of oil shale (OS) and production of energy from it by combustion result in the generation of vast amounts of oil shale ash (OSA). In OSA, more than 40 different mineral phases were identified by X-ray analyses with the major phases being anhydrite, quartz, periclase, calcite, and wollastonite [1]. In Huadian oil shale kaolinite was identified to be a major mineral in addition to quartz [2]. The content of clay minerals, rather than the organic matter, in OS is the main factor determining the mineralogy of

* Corresponding author: e-mail *li@uwp.edu*

OSA, while more lime was produced when the clay minerals content was lower [3]. The major chemical compounds of OSA are $SiO_2$, $Al_2O_3$, $Fe_2O_3$, CaO, MgO, $Na_2O$, and $K_2O$, accounting for 95%, with minor amounts of $K_2O$, $Na_2O$, $SO_3$, $P_2O_5$, and other trace elements [4].

Disposal of OSA is expensive and is associated with serious environmental problems. Therefore, investigations are needed to provide safe disposal and reuse of OSA [5]. Replacement of part of cement by OSA up to 20% did not deteriorate its binding properties, suggesting one possibility for OSA utilization [5]. OSA could be used to synthesize ultrafine silica powders and silica gels by fluidized bed drying of wet-gel slurry at ambient pressure with the properties of the obtained silica powders superior to those of silica powders dried in the furnace [6, 7]. By alkali hydrothermal activation using sodium hydroxide OSA was successfully converted into zeolite, which resulted in the adsorption capacity of lead and cadmium of 70 and 96 mg/g, respectively [8]. The high content of free lime in OSA could be utilized for precipitation of calcium carbonate [9].

Use of OSA-based adsorbents has also been extensively studied. An adsorbent made of OSA after alkali hydrothermal activation using sodium hydroxide had an adsorption capacity of 9 and 12 mg/g for the removal of lead and cadmium ions from aqueous solutions, respectively [10]. The maximum loading capacity of pesticides Deltamethrin and Lambda-Cyhalothrin from aqueous solutions by OSA was as high as 11.4 and 8.6 mg/g, respectively [11]. Adsorption of 2,4-dichlorophenol (2,4-DCP) onto treated OSA resulted in a capacity of 4.7–7.4 mg/g [12]. OSA also showed a high potential to adsorb reactive dyes from aqueous solutions, the adsorption followed the Langmuir isotherms and the capacities were 100, 140, and 180 mg/g respectively for Drim red, Drim blue, and Drim yellow [13].

In addition to OSA, fly ash (FA) has also been investigated for the removal of reactive dyes and heavy metals. Adsorption of three reactive dyes Remazol Brillant Blue, Remazol Red 133, and Rifacion Yellow HED from aqueous solutions on FA fitted well the Langmuir and Freundlich isotherm models, their adsorption capacities were in the range of 135–180, 47–86 and 37–61 mg/g, respectively [14]. FA from coal modified by hydrothermal treatment using NaOH solutions under various conditions could effectively absorb heavy metals and methylene blue (MB), the adsorption capacity of MB reached $5 \times 10^{-5}$ mol/g and the adsorption isotherm followed the Langmuir and Freundlich isotherms [15]. Both basic (cationic) and acid (anionic) dyes can be adsorbed onto the FA produced from brown coal with the sorption capacities in the range of $10^{-1}$–$10^{-3}$ mmol/g, which did not differ significantly for basic and acid dyes [16].

In this study, the removal of MB by using OSA was studied at different physical and chemical parameters such as initial MB concentration, solution pH, temperature, and OSA amounts. The goal of the study was to extend the utilization of OSA waste for the removal of other contaminants from wastewater.

## 2. Experimental

### 2.1. Materials

The oil shale ash (OSA) was obtained from Huadian City, Jilin Province, China. Its major chemical compounds are $SiO_2$, $Al_2O_3$, $Fe_2O_3$, MgO, CaO, and $TiO_2$ (Table 1). The sample was ground to particles less than 100 mesh (150 μm) in size and then ashed at 700 °C for 2 h to ensure no more organic carbon residues. Previous results showed that the leaching rates of aluminum and iron from OSA were low when the calcination temperature was below 700 °C [2]. The mineral morphology in samples was platy before calcination and equilateral after calcination with individual particles in the nanometer range (Fig. 1). The calcinated OSA had a specific surface area of 28 $m^2/g$ and mean pore diameter 3.8 nm as measured in BET analyses. The major mineral phases were quartz, kaolinite, and hematite as revealed by X-Ray diffraction analysis (Fig. 2).

The MB (CAS # 7720-79-3) used was in an HCl form with trihydrate obtained from Tianjin Chemical Co., China. It has no $pK_a$ between pH 0–14 and is in the form $MB^+$ in this pH region. Due to protonation, it is commonly positively charged in water with different resonance forms. MB molecules could form different aggregations at different initial concentrations [17]. Within the tested initial MB concentrations, monomers of MB prevail, and may form mixtures only with dye dimers [17].

**Table 1. Chemical composition of OSA**

| Component | $SiO_2$ | $Al_2O_3$ | $Fe_2O_3$ | CaO | MgO | $TiO_2$ | $Na_2O$ | $K_2O$ |
|---|---|---|---|---|---|---|---|---|
| Wt% | 52.33 | 24.05 | 7.96 | 5.93 | 1.62 | 1.89 | 0.43 | 1.65 |

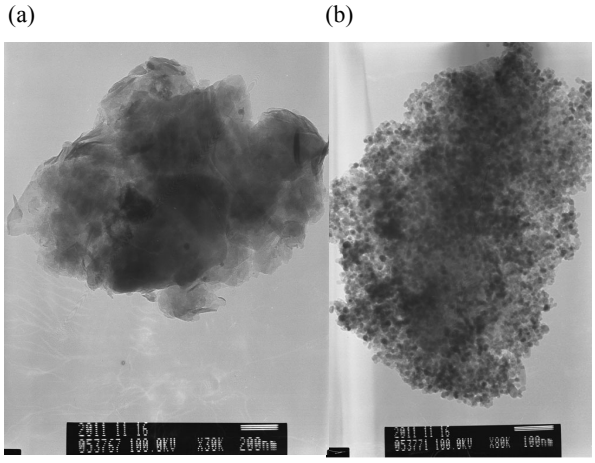


Fig. 1. TEM images of OSA sample: (a) raw, (b) after calcination at 700 °C.

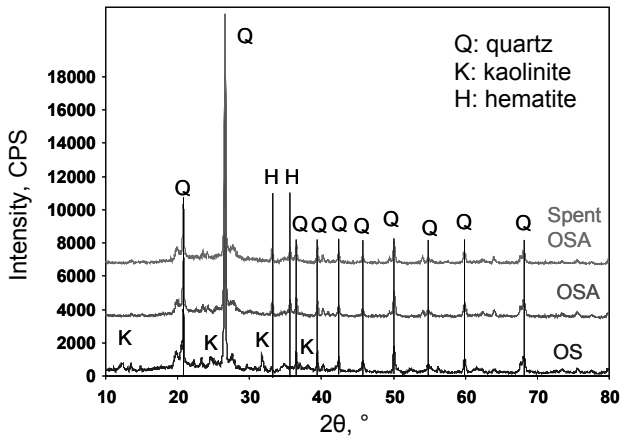


Fig. 2. XRD of OSA samples.

## 2.2. MB adsorption

For MB adsorption study, 3.0 g of OSA was added to 100 mL of MB solutions with initial concentrations from 5 to 80 mg/L, and the mixtures were shaken for 24 h at room temperature. For the pH-dependency test, and adsorption kinetics and temperature effect studies, 0.3 g of OSA was mixed with 100 mL of the MB solution at an initial concentration of 2.5 mg/L. The pH was adjusted to 3–11, the reaction time was from 5 to 240 min, and the temperature was set at 303, 313, 323, and 333 K, respectively. After being shaken at different pH and temperatures for varying amounts of time, the mixture was centrifuged and the supernatants were analyzed for equilibrium MB concentrations by a UV-Vis spectrophotometer.

## 2.3. Instrumental analyses

A Nicolet 380 FT-IR spectrometer (USA) was used for FTIR analyses, and an EM2010 transmission electron microscope (JEOL Corporation, Japan) was used for TEM observation. A DR5000 spectrophotometer (HACH, USA) was used for quantification of MB in solution at a wavelength of 660 nm. A 266S-type pH meter (Orion, USA) was used for pH measurement.

Powder XRD analyses were performed on a PanAnalytical PW3040/60 X-ray diffractometer (Netherlands) with a Ni-filtered Cu Kα radiation at 30 kV and 20 mA. The orientated samples were scanned from 2° to 10° 2θ at 1°/min with a scanning step of 0.01°/step. A 1° divergent slit and scatter slit and a 0.3 mm receiving slit were used.

## 3. Results and discussion

### 3.1. Effect of solution pH on MB adsorption

The pH of the MB aqueous solution was adjusted to 3, 4, 5, 6, 7, 8, 9, 10, and 11, respectively, by adding diluted HCl or NaOH solution. With an increase in solution pH, the adsorption of MB on OSA increased (Fig. 3). Considering that the major mineral phase was quartz, whose negative charge increases as the solution pH increases, while MB is a cationic dye, the increase in MB removal could be attributed to enhanced electrostatic interactions between OSA and $MB^+$. Similarly to OSA, maximum MB removal was observed at pH 8 when coal fly ash (CFA) was used [18]. In contrast, an increase in the initial pH of the solution negatively influenced the sorption of 2,4-DCP on treated OSA [12].

Adsorption of Remazol Brillant Blue on CFA was pH-dependent but those of Remazol Red 133 and Rifacion Yellow HED were not [14]. In contrast, the adsorption of two reactive dyes (Reactive Red 23 and Reactive Blue 171) and two acid dyes (Acid Black 1 and Acid Blue193) from aqueous solution on CFA was pH-dependent with the maximum adsorption capacity at the initial pH of the solution of 7.5–8.5 and 5–6 for reactive and acid dyes, respectively [19]. Sorption of basic dyes on CFA increased at high pH values, whereas the opposite trend was found for acid dyes [16].

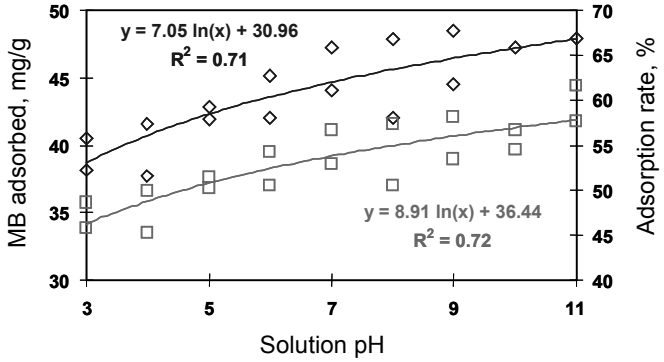


Fig. 3. Effect of solution pH on the amount of MB adsorbed (◇ left y-axis) and rate of MB adsorption (□ right y-axis).

### 3.2. Effect of initial OSA dose on MB adsorption

The rate of MB adsorption, as defined by the percentage of MB removal from solution, increased as the initial OSA dose increased (Fig. 4). However, the amount of MB adsorbed decreased as the dose of OSA increased (Fig. 4). The extent of MB removal decreased with increasing dosage of wheat shells [20].

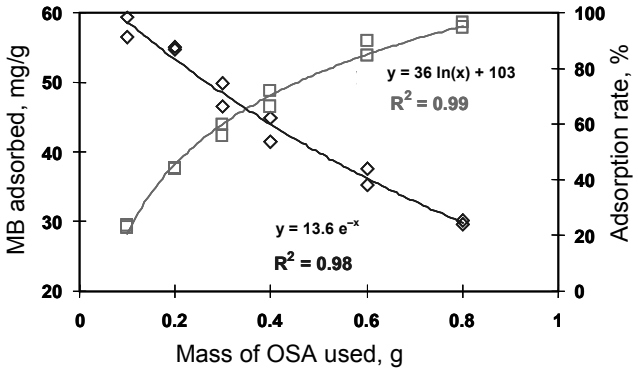


Fig. 4. Effect of the initial OSA dose on the amount of MB adsorbed (◇ left y-axis) and rate of MB adsorption (□ right y-axis).

### 3.3. Effect of temperature on MB adsorption

The adsorption of MB on OSA increases as the temperature increases (Fig. 5). The relationship between $K_d$ (the ratio of the amount of MB adsorbed to the equilibrium MB concentration) and the thermodynamic parameters of adsorption can be expressed as [14, 19]:

$$\ln K_d = -\frac{\Delta H}{RT} + \frac{\Delta S}{R}, \tag{1}$$

where $\Delta H$ is the change in enthalpy, $\Delta S$ is the change in entropy, $R$ is the gas constant, and $T$ is the reaction temperature, K. The free energy of adsorption can be determined by [19]:

$$\Delta G = \Delta H - T\Delta S\,. \tag{2}$$

The calculated thermodynamic parameters are listed in Table 2.

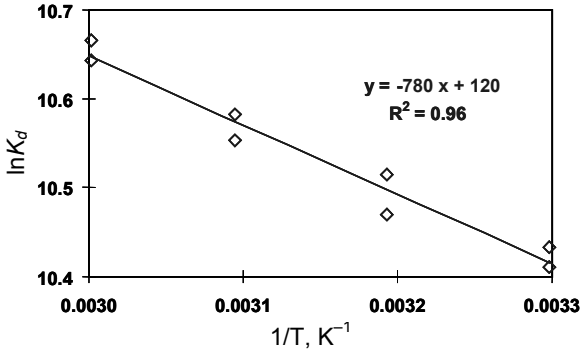


Fig. 5. Influence of temperature on MB adsorption on OSA. The lines are fitted to the observed data based on Eq. (1).

**Table 2. Thermodynamic values of MB adsorption on OSA at different temperatures**

| ln($K_d$), L/kg | | | | ΔG, kJ/mol | | | | ΔH°, kJ/mol | ΔS°, kJ/mol·K |
|---|---|---|---|---|---|---|---|---|---|
| 303 K | 313 K | 323 K | 333 K | 303 K | 313 K | 323 K | 333 K | | |
| 8.83 | 8.89 | 8.97 | 9.06 | –22.3 | –23.2 | –24.1 | –25.1 | 6.4 | 0.1 |

The free energy ($\Delta G$) of MB adsorption on OSA was –22.3, –23.2, –24.1 and –25.1 kJ/mol at 303, 313, 323 and 333 K, respectively, in comparison to –22.6, –24.1 and –26.4 kJ/mol at 303, 313 and 323 K, respectively, for MB adsorption on wheat shells [20]. Compared to the $\Delta G$ value of –8 kJ/mol for TC sorption on silica [21], the higher negative values of $\Delta G$ for MB adsorption on OSA indicated a higher affinity of MB for OSA surfaces. The negative $\Delta G$ value indicates an attractive interaction between MB and OSA, thus a spontaneous adsorption.

The $\Delta H$ and $\Delta S$ for MB adsorption on OSA were 6.4 kJ/mol and 0.1 kJ/mol·K, as against 33.4 kJ/mol and 0.2 kJ/mol·K for MB adsorption on wheat shells [20]. The positive $\Delta H$ value suggests that MB adsorption on OSA is an endothermic process. Therefore, increases in temperature favoured the removal of MB from water by OSA. In contrast, adsorption of 2,4-DCP on the treated residue of Jordanian OS was an exothermic process [12]. As the $K_d$ value for MB adsorption on OSA is much greater than 1 and $\Delta H$ is positive, this resulted in a positive $\Delta S$. The small positive $\Delta S$ indicated that the adsorption resulted in an increase in system randomness as MB molecules were removed from aqueous solution onto the solid surfaces. It may also suggest that the adsorbed MB molecules might adopt a random orientation instead of arranging themselves in an orderly pattern on the external surface of OSA.

### 3.4. Kinetics of MB adsorption on OSA

As the equilibration time increased, the amount of MB increased. The adsorption could attain equilibrium in 2 h (Fig. 6). In comparison, MB adsorption on wheat shells attained equilibrium in 1 h [20]. The adsorption equilibrium of each anionic dye on CFA could be reached within 1 h at respective optimum pH at 293 K [19].

Both the Lagergren first-order and pseudo-second-order adsorption kinetic models were tested to quantify the extent of MB uptake in adsorption kinetics. The pseudo-second-order adsorption kinetic rate equation is expressed as [22]:

$$\frac{t}{q_t} = \frac{1}{k_2 q_e^2} + \frac{1}{q_e} t \,, \tag{3}$$

where $k_2$ (g/mg·h) is the rate constant of the pseudo-second-order adsorption, $q_e$ and $q_t$ (mg/g) are the amount of adsorbate adsorbed at the time of equilibrium and at the time $t$, respectively. The MB adsorption on OSA fitted

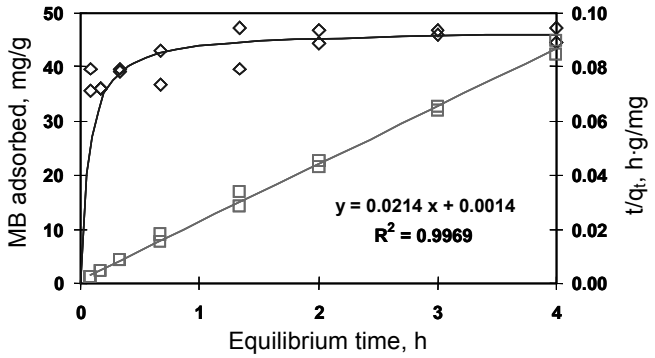


Fig. 6. Effect of contact time on the amount of MB adsorbed (◇ left y-axis) and plot of Eq. (3) (□ right y-axis).

the pseudo-second-order adsorption better (Fig. 6), resulting in the $k_2$ of 0.33 g/mg·h, $q_e$ of 46.7 mg/g, and an initial rate of 714 mg/g·h. Adsorption of MB on CFA fitted both the Lagergren first-order and pseudo-second-order kinetic models and the data followed the pseudo-second-order kinetics well [18]. Similarly, adsorption of MB on wheat shells was described by the pseudo-second-order reaction model [20] and kinetic studies of adsorption of four dyes on CFA followed the pseudo-second-order modal well [19].

Batch kinetic data from experimental investigations on the removal of reactive dyes from aqueous solutions using CFA were well described by external mass transfer and intraparticle diffusion models [14]. Surface adsorption and pore diffusion were attributed to the adsorption mechanisms of MB on CFA with the particle diffusion as the rate-limiting step for the dye removal in the range of 20–60 mg/L [18]. In this study, the smaller particle size minimized the particle diffusion as the rate-limiting step for MB removal, which resulted in a higher initial rate, 714 mg/g·h.

### 3.5. MB adsorption isotherm

Adsorption data for a wide range of adsorbate concentrations are most conveniently described by adsorption isotherms, such as the Langmuir or Freundlich, which relate amounts adsorbed to the equilibrium adsorbate concentration in the bulk fluid phase. The Langmuir isotherm suggests that the adsorbed solute forms a monolayer coverage on the adsorbent surface and there is no interaction between the adsorbed molecules. The linear form of the Langmuir isotherm is described by [23]:

$$\frac{C_L}{C_S} = \frac{1}{K_L S_m} + \frac{C_L}{S_m}, \tag{4}$$

where $C_L$ is the solution concentration at equilibrium (mg/L), $C_S$ is the amount adsorbed at equilibrium (mg/g), $K_L$ is the Langmuir constant (L/mg)

which can be considered as a measurement of the adsorption energy, $S_m$ is the adsorption capacity (mg/g) corresponding to complete monolayer coverage. A plot of $C_L/C_S$ versus $C_L$ over the entire concentration range produces a straight line, which indicates the applicability of the Langmuir isotherm to the system under consideration.

The Freundlich model assumes that different sites with several adsorption energies are involved in the adsorption process. The Freundlich isotherm is expressed by the following equation:

$$C_S = K_F C_L^{1/n}. \tag{5}$$

The linear form of Equation (5) can be written as:

$$\ln C_S = \ln K_F + \frac{1}{n} \ln C_L, \tag{6}$$

where $K_F$ and $n$ are the Freundlich constants related to the adsorption capacity and adsorption intensity, respectively [24]. The intercept and the slope of the linear plot at given experimental conditions provide the values of $K_F$ and $1/n$, respectively.

Fitting of MB adsorption data to both models can be seen in Figure 7. The Freundlich model has slightly higher $R^2$ values than the Langmuir model. The Freundlich isotherm described the equilibrium adsorption data of acid dyes on CFA better than the Langmuir isotherm [19]. In contrast, MB adsorption on montmorillonite followed the Langmuir isotherm [25–28]. The Langmuir isotherm also provided a better fit to the experimental data than the Freundlich isotherm for MB adsorption on a phosphorous rock [29] and on palygorskite [30]. Adsorption of MB on these swelling clays was attributed to cation exchange [28, 31].

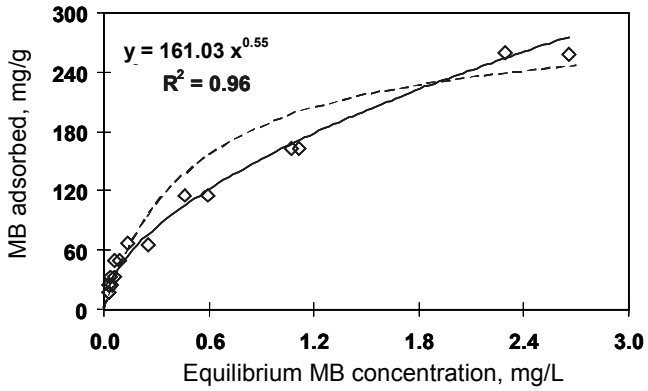


Fig. 7. Isotherm of MB adsorption on OSA. The solid and dashed lines represent the Freundlich and Langmuir fits to the experimental data, respectively.

The adsorption capacity of MB reached 250 mg/g. This value is significantly higher than 100, 140 and 180 mg/g respectively for Drim red, Drim blue and Drim yellow on OSA [13]. In comparison, adsorption of MB on CFA followed the Langmuir isotherm well with a monolayer sorption capacity of 5.7 mg/g [18]. The adsorption capacity of MB on wheat shells amounted to 17, 21 and 22 mg/g at 303, 313 and 323 K, respectively [20]. The adsorption capacity for Reactive Red 23, Reactive Blue 171, Acid Blue193 and Acid Black 1 was 2.1, 1.9, 10.9 and 10.3 mg/g, respectively [19], while the adsorption capacity of 2,4-DCP onto treated OSA was 4.7–7.4 mg/g [12]. The high adsorption capacity of MB and the higher initial rate of MB removal by OSA suggest a potential use of OSA for dye removal from wastewater.

### 3.6. FTIR analyses

The FTIR spectra of MB, raw OS, OSA and OSA-adsorbed MB are plotted in Figure 8. The vibration bands of MB matched with the published data well [32]. The major vibration bands were in the wave number region of 1100 to 1700 $cm^{-1}$. Most of the band positions remained the same after MB adsorption on OSA. The detection of strong bands related to the –C=C– and –C=N– stretching in the polyheterocycles at 1595 $cm^{-1}$ and the –C–N– stretching at 1333 $cm^{-1}$ would suggest that the transition moments of –C=C–

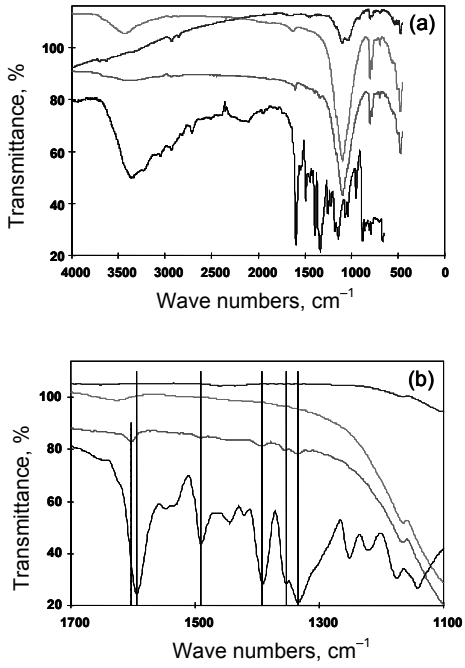


Fig. 8. FTIR spectra of MB (black), OS (blue), OSA (magenta), and OSA-adsorbed MB (red) in 450–4000 (a) and 1100–1700 $cm^{-1}$ (b) regions.

and –C=N– stretching oriented perpendicular to the stainless steel surface [33]. In this study, both strong bands were detected and the 1595 $cm^{-1}$ band blue-shifted to 1600 $cm^{-1}$ after MB adsorption on OSA (Fig. 8b), suggesting a nearly perpendicular orientation of MB molecules to the OSA surface.

## 4. Conclusions

The adsorptive removal of MB by using OSA as sorbent seems promising for utilization of this waste on the one hand and for obtaining higher affinity for color dyes on the other hand. The thermodynamic parameter values showed the adsorption of MB on OSA to be a spontaneous and endothermic process. The Langmuir and Freundlich models fitted the adsorption equilibrium of MB well with the adsorption capacity as high as 250 mg/g. Removal of MB by OSA was relatively fast and equilibrium could be achieved in 2 h. Although the physical process was dominated by the adsorptive removal of MB by OSA, the higher adsorption capacity of MB and its higher initial removal rate were attributed to the nanometer range particle size and larger surface area.

## Acknowledgments

This work was financially supported by the Fundamental Research Funds for the Central Universities of China (No. 2652013107), the Science and Technology Project and the Laboratory Open Funds of China University of Geosciences, Beijing.

## REFERENCES

1. Paat, A., Traksmaa, T. Investigation of the mineral composition of Estonian oil-shale ash using X-Ray diffractometry. *Oil Shale*, 2002, **19**(4), 373–386.
2. Xu, Y.-M., He, D.-M., Wang, D.-M., Lian, Y.-H., Guan, J., Zhang, Q.-M. Influence of calcination temperature on leaching rate of aluminum and iron impurities in oil shale ash. *Oil Shale*, 2009, **26**(2), 163–168.
3. Yoffe, O., Nathan, Y., Wolfarth, A., Cohen, S., Shoval, S. The chemistry and mineralogy of the Negev oil shale ashes. *Fuel*, 2002, **81**(9), 1101–1117.
4. Zhang, L.-D., Zhang, X., Li, S.-H., Wang, Q. Comprehensive utilization of oil shale and prospect analysis. *Energy Procedia*, 2012, **17**(A), 39–43.
5. Al-Hamaiedh, H., Maaitah, O., Mahadin, S. Using oil shale ash in concrete binder. *The Electronic Journal of Geotechnical Engineering* (*EJGE*), 2004, **15**, 601–608.
6. Gao, G.-M., Zou, H.-F., Liu, D.-R., Miao, L.-N., Gan, S.-C., An, B.-C., Xu, J.-J., Li, G.-H. Synthesis of ultrafine silica powders based on oil shale ash by fluidized bed drying of wet-gel slurry. *Fuel*, 2009, **88**(7), 1223–1227.

7. Gao, G.-M., Liu, D.-R., Zou, H.-F., Zou, L.-C., Gan, S.-C. Preparation of silica aerogel from oil shale ash by fluidized bed drying. *Powder Technol.*, 2010, **197**(3), 283–287.
8. Shawabkeh, R., Al-Harahsheh, A., Hami, M., Khlaifat, A. Conversion of oil shale ash into zeolite for cadmium and lead removal from wastewater. *Fuel*, 2004, **83**(7–8), 981–985.
9. Velts, O., Uibu, M., Rudjak, I., Kallas, J., Kuusik, R. Utilization of oil shale ash to prepare PCC: leachibility dynamics and equilibrium in the ash-water system. *Energy Procedia*, 2009, **1**, 4843–4850.
10. Zhu, B.-L., Xiu, Z.-M., Liu, N., Bi, H.-T., Lv, C.-X. Adsorption of lead and cadmium ions from aqueous solutions by modified oil shale ash. *Oil Shale*, 2012, **29**(3), 268–278.
11. Al-Qodah, Z., Shawaqfeh, A. T., Lafi, W. K. Adsorption of pesticides from aqueous solutions using oil shale ash. *Desalination*, 2007, **208**, 294–305.
12. Al-Asheh, S., Banat, F., Masad, A. Use of activated oil shale for the removal of 2,4-dichlorophenol from aqueous solutions. *Water Qual. Res. J. Can.*, 2005, **40**(2), 211–221.
13. Al-Qodah, Z. Adsorption of dyes using shale oil ash. *Water Res.*, 2000, **34**(17), 4295–4303.
14. Dizge, N., Aydiner, C., Demirbas, E., Kobya, M., Kara, S. Adsorption of reactive dyes from aqueous solutions by fly ash: Kinetic and equilibrium studies. *J. Hazard. Mater.*, 2008, **150**(3), 737–746.
15. Wang, S., Soudi, M., Li, L., Zhu, Z. H. Coal ash conversion into effective adsorbents for removal of heavy metals and dyes from wastewater. *J. Hazard. Mater.*, 2006, **133**(1–3), 243–251.
16. Janõs, P., Buchtová, H., Rýznarová, M. Sorption of dyes from aqueous solutions onto fly ash. *Water Res.*, 2003, **37**(20), 4938–4944.
17. Klika, Z., Čapková, P., Horáková, P., Valášková, M., Malý, P., Macháň, R., Pospíšil, M. Composition, structure, and luminescence of montmorillonites saturated with different aggregates of methylene blue. *J. Colloid Interf. Sci.* 2007, **311**(1), 14–23.
18. Kumar, K. V., Ramamurthi, V., Sivanesan, S. Modeling the mechanism involved during the sorption of methylene blue onto fly ash. *J. Colloid Interf. Sci.*, 2005, **284**(1), 14–21.
19. Sun, D.-S., Zhang, X.-D., Wu, Y.-D., Liu, X. Adsorption of anionic dyes from aqueous solution on fly ash. *J. Hazard. Mater.*, 2010, **181**(1–3), 335–342.
20. Bulut, Y., Aydin, H. A kinetics and thermodynamics study of methylene blue adsorption on wheat shells. *Desalination*, 2006, **194**, 256–267.
21. Turku, I., Sainio, T., Paatero, E. Thermodynamics of tetracycline adsorption on silica, *Environ. Chem. Lett.*, 2007, **5**(4), 225–228.
22. Ho, Y. S., McKay, G. Pseudo-second order model for sorption processes. *Process Biochem.*, 1999, **34**(5), 451–465.
23. Machado, N. R. C. F., Miotto, D. M. M. Synthesis of Na–A and –X zeolites from oil shale ash. *Fuel*, 2005, **84**(18), 2289–2294.
24. Pollard, S. J. T., Sollars, C. J., Perry, R. A low cost adsorbent from spent bleaching earth. I – The selection of an activation procedure. *J. Chem. Technol. Biot.*, 1991, **50**(2), 265–275.
25. Chen, G., Pan, J., Han, B., Yan, H. Adsorption of methylene blue on montmorillonite. *J. Disper. Sci. Technol.*, 1999, **20**(4), 1179–1187.

26. El Mouzdahir, Y., Elmchaouri, A., Mahboub, R., Gil, A., Korili, S. A. Adsorption of methylene blue from aqueous solutions on a Moroccan clay. *J. Chem. Eng. Data*, 2007, **52**, 1621–1625.
27. Almeida, C. A. P., Debacher, N. A., Downs, A. J., Cottet, L., Mello, C. A. D. Removal of methylene blue from colored effluents by adsorption on montmorillonite clay. *J. Colloid Interf. Sci.*, 2009, **332**(1), 46–53.
28. Li, Z., Chang, P.-H., Jiang, W.-T., Jean, J.-S., Hong, H. Mechanism of methylene blue removal from water by swelling clays. *Chem. Eng. J.*, 2011, **168**(3), 1193–1200.
29. Malash, G. F., El-Khaiary, M. I. Methylene blue adsorption by the waste of Abu-Tartour phosphate rock. *J. Colloid Interf. Sci.*, 2010, **348**(2), 537–545.
30. Al-Futaisi, A., Jamrah, A., Al-Hanai, R. Aspects of cationic dye molecule adsorption to palygorskite. *Desalination*, 2007, **214**, 327–342.
31. Rytwo, G., Serban, C., Nir, S., Margulies, L. Use of methylene blue and crystal violet for determination of exchangeable cations in montmorillonite. *Clays Clay Miner.*, 1991, **39**(5), 551–555.
32. Ovchinnikov, O. V., Chernykh, S. V., Smirnov, M. S., Alpatova, D. V., Vorob'eva, R. P., Latyshev, A. N., Evlev, A. B., Utekhin, A. N., Lukin, A. N. Analysis of interaction between the organic dye methylene blue and the surface of AgCl(I) microcrystals. *J. Appl. Spectrosc.*, 2007, **74**(6), 809–816.
33. Imamura, K., Ikeda, E., Nagayasu, T., Sakiyama, T., Nakanishi, K. Adsorption behavior of methylene blue and its congeners on a stainless steel surface. *J. Colloid Interf. Sci.*, 2002, **245**(1), 50–57.

*Presented by S. Li*
Received August 25, 2013